Late Transition-Metal Sulfido Complexes: Reactivity Studies and Mechanistic Analysis of Their Conversion into Metal–Sulfur Cubane Complexes

Daniel A. Dobbs and Robert G. Bergman*

Department of Chemistry, University of California, Berkeley, California 94720

Received March 30, 1994[⊗]

Bimetallic bridging sulfur complexes having the general structure $Cp^*M(PR_3)S_2IrCp^*$ (**3**, R = Me, M = Ir; **12**, R = Me, M = Rh; **15**, R = *p*-tolyl, M = Ir) have been prepared. Heating these compounds leads to the metalla–sulfur cubane complexes $(Cp^*MS)_2(Cp^*IrS)_2$ (**10**, M = Ir; **13**, M = Rh). The observation that diiridium/dirhodium complex **13** is the only product obtained quantitatively from the thermolysis of **12** provides evidence that the dimeric units remain intact on the pathway to cubane formation rather than dissociating to monomeric units followed by reassembly into the tetramer. A mechanistic study of the cubane-assembly reaction was undertaken using complex **15**. The reaction is first-order in [**15**] and zero-order in [PR_3] when the concentration of phosphine is low. At high (flooding) [PR_3], the rate is second-order in [**15**] and inverse second-order in phosphine concentration. These data are consistent with a mechanism in which a doubly unsaturated intermediate, $Cp^*MS_2IrCp^*$, is generated by reversible loss of phosphine and then in a second bimolecular step dimerizes to form the cubane. The reactions of **3** with methyl bromide, carbon monoxide, and *tert*-butyl isocyanide are also described. The single crystal X-ray structures of $Cp^*Ir(PMe_3)S_2IrCp^*$ (**3**), $Cp^*Ir(CN\text{-}t\text{-}Bu)(\mu\text{-}S)_2Ir(CN\text{-}t\text{-}Bu)Cp^*$ (**9**), and $(Cp^*IrS)_4$ (**10**) have been determined. Complex **3** crystallized in the monoclinic system, space group $P2_1$ with $a = 8.556(1)$ Å, $b = 14.093(2)$ Å, $c = 10.977(2)$ Å, $\beta = 103.28(1)°$, and $Z = 2$. Refinement by standard least-squares techniques gave final residuals $R = 0.039$ and $R_w = 0.046$. Complex **9** crystallized in the monoclinic system, space group $C2/c$ with $a = 18.798(5)$ Å, $b = 9.554(2)$ Å, $c = 18.219(3)$ Å, $\beta = 90.34°$, and $Z = 8$. Refinement by standard least-squares techniques gave final residuals $R = 0.034$ and $R_w = 0.040$. Complex **10** crystallized in the orthorhombic system, space group $I\bar{4}$ with $a = 12.026(3)$ Å, $b = 12.026(3)$ Å, $c = 14.844(3)$ Å, and $Z = 2$. Refinement by standard least squares techniques gave final residuals $R = 0.031$ and $R_w = 0.039$.

Metal–sulfur clusters are central components of the active sites of enzymes such as ferredoxin and nitrogenase.[1–4] Such complexes also have been studied extensively because of their relevance to metal-catalyzed hydrodesulfurization.[5,6] An important aspect in modeling and understanding the key processes involved in these systems has been the rational synthesis of heterometallic cluster complexes, especially sulfur cubane complexes.[7–18] Despite many studies in this area, little mechanistic information has been obtained about the formation of higher molecularity sulfur complexes from simple precursors.[19] Early examples of cluster formation were presumed to proceed by "self-assembly" type mechanisms, whereby small metal-sulfur fragments assemble into higher molecularity systems through stepwise oligomerization.[20]

We undertook a study of late transition-metal sulfido complexes in order to understand better the factors that control the aggregation of these complexes. We report here the preparation of binuclear iridium and rhodium sulfido complexes, their conversion to metal–sulfur cubane complexes, and mechanistic studies of these cubane-forming reactions. We also report ligand exchange reactions and reactions at the sulfur bridges of binuclear iridium sulfido complexes.[21]

Results and Discussion

Deprotonation of a (Hydrosulfido)chloroiridium Complex. Because few examples of late transition metal compounds containing a terminal sulfido functionality have been reported,[22] we sought the synthesis of such a complex. Terminal imido and terminal carbene complexes of iridium have been synthesized recently suggesting that terminal sulfido complexes may

[⊗] Abstract published in *Advance ACS Abstracts,* October 1, 1994.

(1) Stack, T. D. P.; Holm, R. H. *J. Am. Chem. Soc.* **1988**, *110*, 2484–2494.
(2) Palermo, R. E.; Singh, R.; Bashkin, J. K.; Holm, R. H. *J. Am. Chem. Soc.* **1984**, *106*, 2600–2612.
(3) Berg, J. M.; Holm, R. H. *Metal Ions in Biology*; Interscience: New York, 1982; Vol. 4.
(4) Ibers, J. A.; Holm, R. H. *Science* **1980**, *209*, 223–235 and references therein.
(5) Chen, J.; Daniels, L. M.; Angelici, R. J. *J. Am. Chem. Soc.* **1990**, *112*, 199–204 and references therein.
(6) Spies, G.; Angelici, R. J. *Organometallics* **1987**, *6*, 1897–1903.
(7) Kuwata, S.; Mizobe, Y.; Hidai, M. *J. Am. Chem. Soc.* **1993**, *115*, 8499–8500.
(8) Riaz, U.; Curnow, O.; Curtis, M. D. *J. Am. Chem. Soc.* **1991**, *113*, 1416–1417.
(9) Nianyong, Z.; Yifan, Z.; Xintao, W. *J. Chem. Soc., Chem. Commun.* **1990**, 780–781.
(10) Inomata, S.; Tobita, H.; Ogino, H. *J. Am. Chem. Soc.* **1990**, *112*, 6145–6146.
(11) Shibahara, T.; Akashi, H.; Kuroya, H. *J. Am. Chem. Soc.* **1986**, *108*, 1342–1343.
(12) Halbert, T. R.; Cohen, S. A.; Stiefel, E. I. *Organometallics* **1985**, *4*, 1689–1690.
(13) Brunner, H.; Janietz, N.; Wachter, J.; Zahn, T.; Ziegler, M. L. *Angew. Chem., Int. Ed. Engl.* **1985**, *24*, 133–135.
(14) Brunner, H.; Kauermann, H.; Wachter, J. *J. Organomet. Chem.* **1984**, *265*, 189–198.
(15) Brunner, H.; Kauermann, H.; Wachter, J. *Angew. Chem., Int. Ed. Engl.* **1983**, *22*, 549–550.
(16) Brunner, H.; Wachter, J. *J. Organomet. Chem.* **1982**, *240*, C41–C44.
(17) Williams, P. D.; Curtis, M. D.; Duffy, D. N.; Butler, W. M. *Organometallics* **1983**, *2*, 165–167.
(18) Curtis, M. D.; Williams, P. D. *Inorg. Chem.* **1983**, *22*, 2661–2662.
(19) Rauchfuss, T. B.; Weatherill, T. D.; Wilson, S. R.; Zebrowski, J. P. *J. Am. Chem. Soc.* **1983**, *105*, 6508–6509.
(20) Holm, R. H. *Chem. Soc. Rev.* **1981**, *10*, 455–491.
(21) A preliminary report of this work has been published: Dobbs, D. A.; Bergman, R. G. *J. Am. Chem. Soc.* **1992**, *114*, 6908–6909.
(22) A monomeric rhodium sulfido species has been postulated as an intermediate in the formation of a bridging complex; see: Wachter, J. *Angew. Chem., Int. Ed. Engl.* **1989**, *28*, 1613–1626.

0020-1669/94/1333-5329$04.50/0

Scheme 1

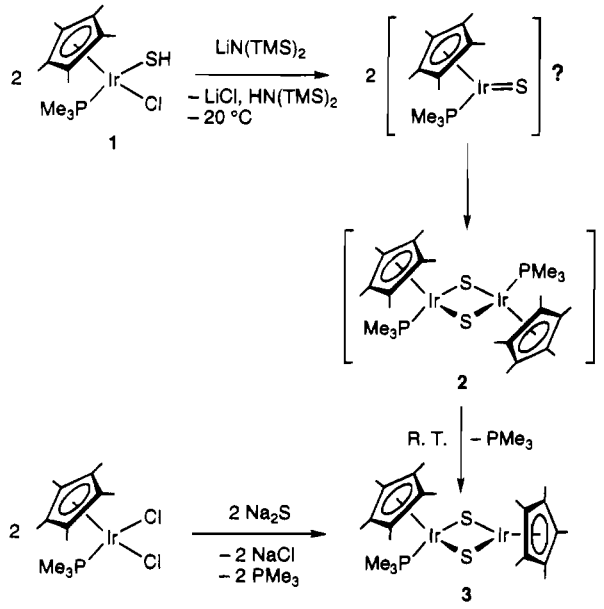

1 2 3

also be stable.[23-25] Because deprotonation of a (hydrosulfido)-halozirconium complex led to the production of a terminal zirconium sulfido species,[26] we reasoned that addition of the strong base lithium hexamethyldisilazane to Cp*Ir(PMe$_3$)(SH)-Cl (**1**) might result in deprotonation of the thiol group with subsequent loss of LiCl to produce the corresponding terminal sulfido complex Cp*(PMe$_3$)Ir=S (Scheme 1). (Hydrosulfido)-chloroiridium complex **1** was therefore treated with lithium hexamethyldisilazane in d_8-toluene at low temperature (−20 °C). This produced a deep red complex which was found to be stable in solution only at low temperatures. Monitoring the transformation by ^{1}H NMR spectroscopy at −20 °C showed that this complex displayed resonances consistent with a species containing a pentamethylcyclopentadienyl moiety and a PMe$_3$ ligand bound to iridium.

The most likely formulation for this metastable red complex is [Cp*(PMe$_3$)IrS]$_n$. However, low temperature experiments with trapping reagents expected to react with a terminal sulfido species such as acetylenes, isocyanides, CO_2, and COS did not give detectable amounts of adducts. We therefore believe this complex is not a monomeric sulfido species but is likely a dimer Cp*Ir(PMe$_3$)(μ-S)$_2$Ir(PMe$_3$)Cp* (**2**) (Scheme 1). This formulation is based on its simple ^{1}H NMR spectrum, its relative unreactivity toward trapping reagents, and its red color, which is a characteristic of other bridging sulfido complexes with ligands on each of the metal centers (*vide infra*).[27] This complex may form by the dimerization of a terminal sulfido intermediate.[28,29]

The dimeric complex Cp*Ir(PMe$_3$)(μ-S)$_2$Ir(PMe$_3$)Cp* (**2**) proposed above proved to be unstable: upon warming the sample to 25 °C a new green complex Cp*Ir(PMe$_3$)(μ-S)$_2$IrCp*

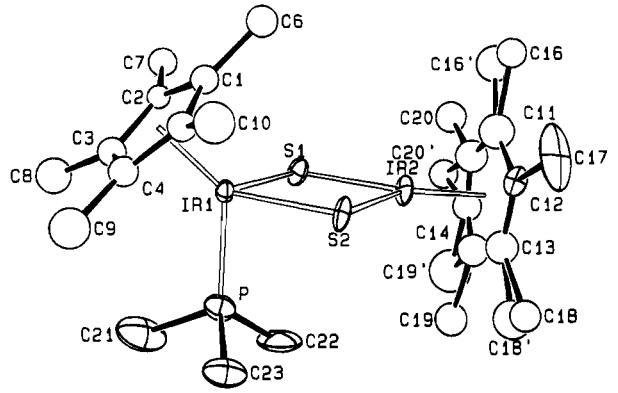

Figure 1. ORTEP diagram of compound **3**. Thermal ellipsoids are at the 50% probability level.

Table 1. Crystal and Data Collection Parameters[a]

	compound		
	3	**9**	**10**
temp (°C)	−95	−95	−110
empirical formula	$Ir_2S_2PC_{23}H_{39}$	$Ir_2N_2S_2C_{15}H_{24}$	$Ir_4S_4C_{40}H_{60}$
fw	795.1	885.2	1438.0
space group	$P2_1$	$C2/c$	$I\bar{4}$
a (Å)	8.556(1)	18.798(5)	12.026(3)
b (Å)	14.093(2)	9.554(2)	12.026(3)
c (Å)	10.977(2)	18.219(3)	14.844(3)
α (deg)	90.0	90.0	90.0
β (deg)	103.28(1)	90.34	90.0
γ (deg)	90.0	90.0	90.0
V (Å^3)	1288.2(7)	3272(2)	2146.8(16)
Z	2	8	2
μ (cm^{-1})	105.1	82.4	125.3
$R(F)$ (%)	3.9	3.4	3.1
$R_w(F)$ (%)	4.6	4.3	3.9

[a] Parameters common to all structures: Radiation, Mo Kα (λ = 0.709 26 Å except for **9** in which λ = 0.710 73 Å); monochromator, highly-oriented graphite (2θ = 12.2°); detector, crystal scintillation counter, with PHA; 2θ range, 3−45°; scan type, θ−2θ; background, measured over 0.25($\Delta\theta$) added to each end of the scan; intensity standards, measured every 1 h of X-ray exposure time; orientation, 3 reflections checked after every 200 measurements. [b] Unit cell parameters and their esd's were derived by a least-squares fit to the setting angles of the unresolved Mo Kα components of 24 reflections with the given 2θ range. In this and all subsequent tables the esd's of all parameters are given in parentheses, right-justified to the least significant digit(s) of the reported value.

(**3**) was produced along with 1 equiv of PMe$_3$.[30-33] The structure of the iridium sulfido complex **3** was confirmed by X-ray diffraction. An ORTEP diagram is included in Figure 1. Crystal and data collection parameters are found in Table 1. The Ir(1)−S distance at the formally 18-electron iridium center of 2.340(5) (ave) Å is significantly longer than the Ir-(2)−S distance of 2.268(5) (ave). This difference in bond length may be attributed to π-orbital donation of the lone pairs from the sulfur atoms to the electron deficient iridium center Ir(2). The angles S−Ir(1)−S and Ir(1)−S−Ir(2) are 77.2(2) and 100.4-(2)°, respectively. Selected interatomic distances and angles are given in Tables 2 and 3, respectively.

(23) Michelman, R. I.; Bergman, R. G.; Andersen, R. A. *Organometallics* **1993**, *12*, 2741−2751.
(24) Glueck, D. S.; Wu, J.; Hollander, F. W.; Bergman, R. G. *J. Am. Chem. Soc.* **1991**, *113*, 2041−2060.
(25) Klein, D.; Bergman, R. G. *J. Am. Chem. Soc.* **1989**, *111*, 3079−3080.
(26) Carney, M. J.; Walsh, P. J.; Hollander, F. J.; Bergman, R. G. *Organometallics* **1992**, *11*, 761−777.
(27) The use of sterically bulky phosphines in this reaction led to intractable materials.
(28) For a similar ruthenium dimer, see: Koelle, U.; Rietmann, C.; Engler, T. U. *J. Organomet. Chem.* **1992**, *423*, C20 and the reference immediately following.
(29) Hornig, A.; Rietmann, C.; Englert, U.; Wagner, T.; Kölle, U. *Chem. Ber.* **1993**, *126*, 2609.
(30) For other late transition metal bridging sulfido species, see: Lockemeyer, J. R.; Rauchfuss, T. B.; Rheingold, A. L. *J. Am. Chem. Soc.* **1989**, *111*, 5733−5738, and references therein. Also see the following three references.
(31) Bright, T. A.; Jones, R. A.; Koschmieder, S. U.; Nunn, C. M. *Inorg. Chem.* **1988**, *27*, 3819−3825.
(32) A bridging monosulfido rhodium complex Cp*Rh(CO)(μ-S)Rh(CO)-Cp* has been isolated from the reaction of Cp*Rh(CO)$_2$RhCp* with S_8; see: Brunner, H.; Janietz, N.; Meier, W.; Wachter, J.; Herdtweck, E.; Herrmann, W. A.; Serhadli, O.; Ziegler, M. L. *J. Organomet. Chem.* **1988**, *347*, 237−252.
(33) Bianchini, C.; Mealli, C.; Meli, A.; Sabat, M. *Inorg. Chem.* **1986**, *25*, 4617−4618.

Table 2. Selected Interatomic Distances (Å) for **3**

Ir1–S1	2.317(4)	Ir1–Ir2	3.568(1)
Ir1–S2	2.363(5)	Ir2–S1	2.273(5)
Ir1–P	2.251(5)	Ir2–S2	2.262(5)
Ir1–Cp1	2.177(17)	Ir2–Cp2	1.797

Table 3. Selected Interatomic Angles (deg) for **3**

Cp1–Ir1–S1	125.12	Cp2–Ir2–S1	136.16
Cp1–Ir1–S2	125.65	Cp2–Ir2–S2	142.06
Cp1–Ir1–P	132.69	S1–Ir2–S2	81.12(14)
S1–Ir1–S2	77.22(15)	Ir1–S1–Ir2	100.44(17)
S1–Ir1–P	92.06(18)	Ir1–S2–Ir2	101.19(16)
S2–Ir1–P	86.89(16)		

Scheme 2

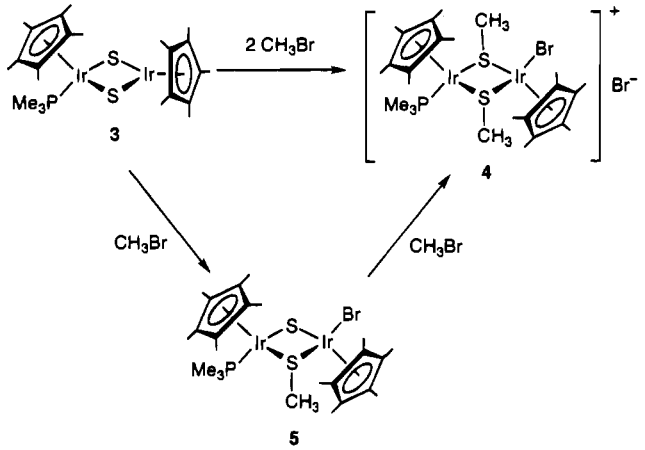

In order to facilitate reactivity studies of binuclear sulfido complex **3**, it was synthesized on a large scale by an alternative method. Treatment of $Cp^*Ir(PMe_3)Cl_2$ with 2 equiv of sodium sulfide in acetonitrile produced a green solution of complex **3** which was isolated in 72% yield after chromatography on alumina III (Scheme 1). This procedure has the advantage of producing **3** directly from the iridium dichloride and thus avoids several intermediate steps.

Reactivity of Binuclear Sulfido Complex 3. The nucleophilicity of binuclear sulfido complex **3** was examined by reaction with methyl bromide. When treated with 2 equiv of methyl bromide, complex **3** produced the dimethylated cationic complex $[Cp^*Ir(PMe_3)(\mu\text{-}SMe)_2Ir(Br)Cp^*]^+Br^-$ (**4**) within minutes at room temperature as light yellow crystals in 89% yield (Scheme 2). A molar conductivity measurement of this complex in acetonitrile was consistent with a 1:1 electrolyte.[34] This reaction is likely the result of nucleophilic attack of the sulfido bridges on methyl bromide. The addition of 1 equiv of methyl bromide resulted primarily in a complex best formulated as the monomethylated complex $Cp^*Ir(PMe_3)(\mu\text{-}SMe)(\mu\text{-}S)Ir(Br)Cp^*$ (**5**) as deep red crystals and small amounts of the dimethylated complex **4** (10:1 mixture of **5**:**4**) from which **5** could not be separated (Scheme 2).

Sulfido dimer **3** was found to be stable when the coordination sphere of only one metal atom is occupied by phosphine. All attempts to coordinate a second phosphine moiety to this complex gave back starting material. Phosphine exchange was observed, however. When complex **3** was treated with excess d_9-PMe_3 at 45 °C, signals attributable to the bound PMe_3 moiety of **3** were observed by ^1H and $^{31}P\{^1H\}$ NMR spectroscopy to decrease in intensity and those due to free PMe_3 emerged, indicating that phosphine exchange had occurred (30% conversion after 24 h).

(34) The typical range for a 1:1 electrolyte in acetonitrile solution is Λ_m = 120–180 Ω^{-1} cm^2 mol^{-1}, we obtained a value of 147 Ω^{-1} cm^2 mol^{-1}. See: Geary, W. J. *Coord. Chem. Rev.* **1971**, *7*, 81–122.

Scheme 3

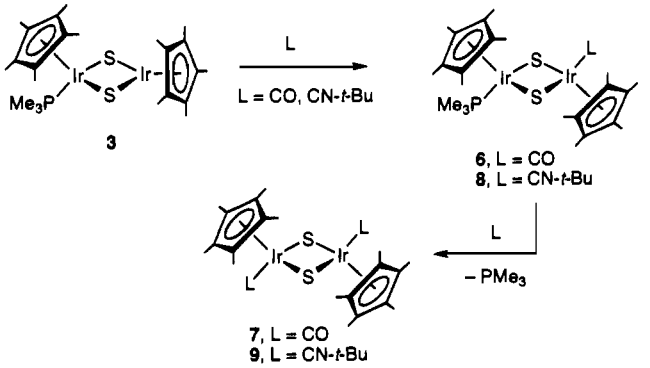

Although the bridging sulfido complex **3** is stable at room temperature with phosphine coordinated to just one of the iridium centers, stable bis-ligand adducts can be formed by addition of carbon monoxide and *tert*-butyl isocyanide. Addition of carbon monoxide to binuclear species **3** at room temperature produced the phosphine monocarbonyl complex $Cp^*Ir(PMe_3)(\mu\text{-}S)_2Ir(CO)Cp^*$ (**6**) (Scheme 3). This terminal carbonyl complex was isolated as red crystals in good yield and was characterized by spectroscopic and analytical methods, including IR spectroscopy (ν_{CO} = 1968 cm^{-1}) and $^{13}C\{^1H\}$ NMR spectroscopy (δ 178.9 for *C*O). Complex **6** was observed to reversibly lose carbon monoxide in toluene at room temperature and re-form starting material but was stable in the solid state and under 1 atm of carbon monoxide in solution. When sulfido complex **3** was heated under 2 atm of carbon monoxide at 85 °C for 2 days, the phosphine was replaced by another 1 equiv of carbon monoxide to form $Cp^*Ir(CO)(\mu\text{-}S)_2Ir(CO)Cp^*$ (**7**).[32] Dicarbonyl complex **7** was isolated in 84% yield as red crystals. In contrast to **6**, this complex does not lose carbon monoxide in solution at room temperature.

In a similar reaction, addition of 1 equiv of *tert*-butyl isocyanide to complex **3** resulted directly in the production of $Cp^*Ir(CN\text{-}t\text{-}Bu)(\mu\text{-}S)_2Ir(CN\text{-}t\text{-}Bu)Cp^*$ (**9**), 1 equiv of PMe_3, and starting material (Scheme 3). Early in the reaction, resonances for an intermediate were observed by ^1H NMR spectroscopy and are consistent with a mono(*tert*-butyl isocyanide) adduct, $Cp^*Ir(PMe_3)(\mu\text{-}S)_2Ir(CN\text{-}t\text{-}Bu)Cp^*$ (**8**). This complex could not be isolated because it reacts rapidly with another 1 equiv of *tert*-butyl isocyanide to lose PMe_3 and generate **9**. In contrast to the carbon monoxide reaction, we believe that the larger tert-butyl isocyanide ligand facilitates dissociation of PMe_3 with subsequent coordination of the second equivalent of *tert*-butyl isocyanide. This is based on the similar observation that the bis-PMe_3-substituted complex **2** is also unstable, presumably due to steric effects, and loses PMe_3 to generate the monophosphine binuclear complex **3**.

The trans geometry of complex **9** was confirmed by an X-ray crystallographic study. An ORTEP diagram is shown in Figure 2. Crystal and data collection parameters are found in Table 1. Selected interatomic distances and angles are found in Tables 4 and 5. The Ir–S distance of 2.376(3) Å compares well with the Ir–S distance observed in $Cp^*Ir(PMe_3)(\mu\text{-}S)_2IrCp^*$ (**3**) for the iridium atom with coordinated phosphine. It therefore appears that the isocyanide ligand's ability to π-back-bond and accept electron density from the iridium atoms has no effect on the Ir–S distances observed.

Cubane Cluster Formation. Heating binuclear complex **3** at 135 °C for 7 days resulted in the loss of PMe_3 and formation of a tetranuclear cubane complex $(Cp^*IrS)_4$ (**10**) in 65% yield (Scheme 4). This complex is isostructural with $(CpCoS)_4$[35] and the rhodium analog $(Cp^*RhS)_4$ which has been prepared

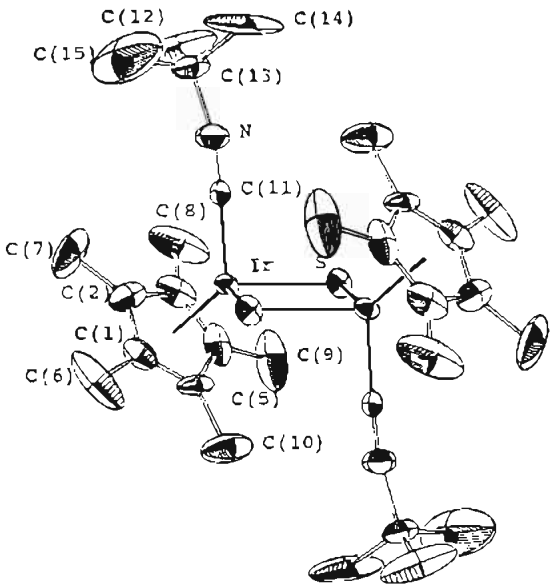

Figure 2. ORTEP diagram of compound **9**. Thermal ellipsoids are at the 50% probability level.

Table 4. Selected Interatomic Distances (Å) for **9**

Ir−S1	2.376(3)	Ir−C11	1.885(10)
Ir−S1′	2.367(2)	N1−C11	1.153(11)
Ir−Cp	1.893(11)		

Table 5. Selected Interatomic Angles for **9**

S1−Ir−S1′	79.32(9)	C11−Ir−Cp	126.9(3)
Ir−S1−Ir′	100.68(9)	C13−N1−C11	169.5(10)
S1−Ir−C11	93.4(3)	N1−C11−Ir	175.6(8)
S1−Ir−Cp	126.83(6)		

Scheme 4

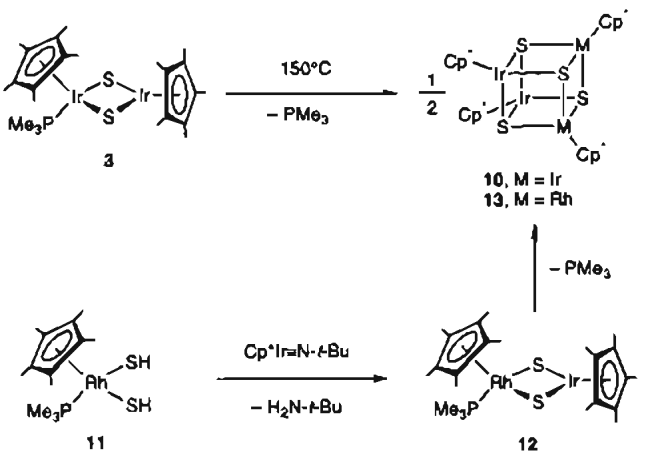

recently.[36] The cubane complex **10** was crystallized directly from the reaction mixture by slow cooling to give red single crystals. An ORTEP diagram is included in Figure 3. Crystal and data collection parameters are found in Table 1, and selected interatomic distances and angles are found in Tables 6 and 7. The structure confirms the tetranuclear core of this complex, and the Ir−S distance of 2.372(3) Å is consistent with those observed in other iridium sulfido complexes presented here.

To gain insight into the cubane assembly reaction, a rhodium−iridium compound isostructural to the bridging sulfido complex **3** was prepared by a different method. Treatment of $Cp^*Rh(PMe_3)(SH)_2$ (**11**)[37] with 1 equiv of $Cp^*Ir{\equiv}N\text{-}t\text{-}Bu$ in

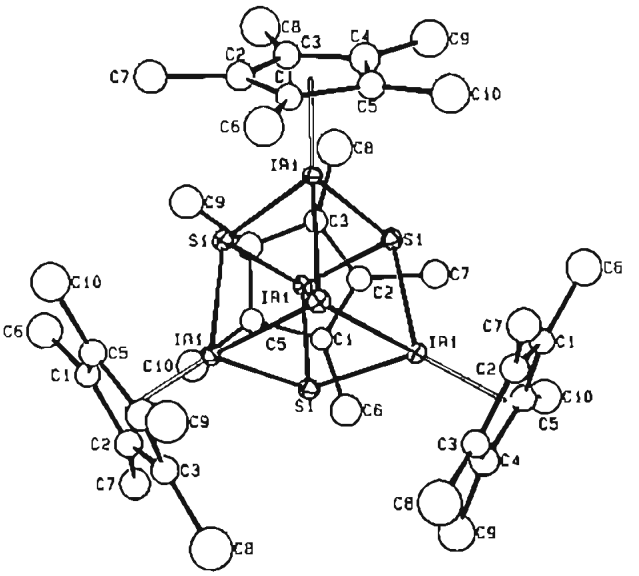

Figure 3. ORTEP diagram of compound **10**. Thermal ellipsoids are at the 50% probability level.

Table 6. Selected Interatomic Distances (Å) for **10**

Ir1−Ir1	3.602(1)	Ir1−S1	2.372(3)
Ir1−Ir1	3.584(1)	Ir1−S1	2.380(3)
Ir1−S1	2.367(3)	Ir1−Cp1	1.818

Table 7. Selected Interatomic Angles (deg) for **10**

S1−Ir1−S1	81.00(12)	Cp1−Ir1−S1	131.08
S1−Ir1−S1	81.30(11)	Ir1−S1−Ir1	98.95(10)
S1−Ir1−S1	81.20(11)	Ir1−S1−Ir1	98.07(11)
Cp1−Ir1−S1	129.72	Ir1−S1−Ir1	97.94(11)

benzene produced $Cp^*Rh(PMe_3)(\mu\text{-}S)_2IrCp^*$ (**12**) in 93% yield along with 1 equiv of *tert*-butylamine (Scheme 4). The structure of **12** was supported by ^1H, $^{13}C\{^1H\}$, and $^{31}P\{^1H\}$ NMR spectroscopy. The $^{31}P\{^1H\}$ NMR spectrum displays one doublet with a Rh−P coupling constant of 165.9 Hz which is consistent with the phosphine moiety bound to rhodium rather than iridium. No evidence for the presence of an isomeric iridium−phosphine form of this complex was observed at room temperature.

Heating the rhodium/iridium binuclear complex **12** to 120 °C for 16 h produced only the tetranuclear complex $(Cp^*IrS)_2(Cp^*RhS)_2$ (**13**) in 53% yield (Scheme 4). An X-ray diffraction study of this complex, although disordered as to the positions of the rhodium and iridium atoms, confirmed the tetranuclear structure. During the course of the reaction, another complex was observed by ^1H and $^{31}P\{^1H\}$ NMR spectroscopy.[38] We propose this to be $Cp^*Ir(PMe_3)(\mu\text{-}S)_2RhCp^*$, the product due to the apparent result of loss of phosphine at rhodium and recoordination at iridium.

Bridging sulfido complexes with a variety of phosphine ligands can be synthesized using the methodology that produced the rhodium/iridium complex **12**. Treatment of $Cp^*Ir(P(p\text{-tolyl})_3)(SH)_2$ (**14**) with 1 equiv of $Cp^*Ir{\equiv}N\text{-}t\text{-}Bu$ produced $Cp^*Ir(P(p\text{-tolyl})_3)(\mu\text{-}S)_2IrCp^*$ (**15**) in 94% yield (Scheme 5). The starting material **14** was prepared in analogy to the method of Klein[37,39] by treatment of $Cp^*Ir(P(p\text{-tolyl})_3)Cl_2$ with 2.5 equiv of sodium hydrogen sulfide in ethanol with a 25-fold excess of

(35) Simon, G. L.; Dahl, L. F. *J. Am. Chem. Soc.* **1973**, *95*, 2164−2174.
(36) Skaugset, A. E.; Rauchfuss, T. B.; Wilson, S. R. *Organometallics* **1990**, *9*, 2875−2876.
(37) Klein, D. P.; Kloster, G. M.; Bergman, R. G. *J. Am. Chem. Soc.* **1990**, *112*, 2022−2024.
(38) This complex displayed the following resonances by NMR spectroscopy: ^1H NMR (C_6D_6) δ 1.68 (d, J = 1.5 Hz, 15H, $C_5Me_5Ir(P)$), 1.59 (s, 15H, C_5Me_5), 1.49 (d, J = 10.2 Hz, 9H, PMe_3); $^{31}P\{^1H\}$-NMR (C_6D_6) d −34.7 (s).
(39) This complex was prepared by a method analogous to that used for $Cp^*Ir(PMe_3)(SH)_2$: Klein, D. P. Unpublished results.

Scheme 5

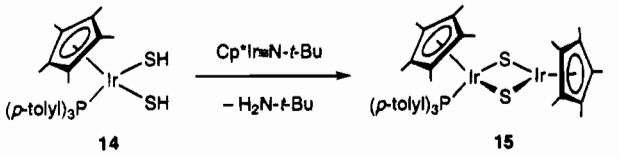

Scheme 6

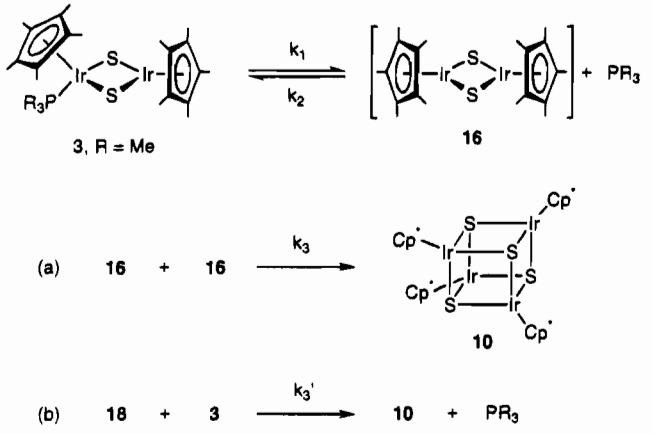

hydrogen sulfide. Bis(hydrosulfido) complex **14** was found to be unstable and, therefore, was used as soon as prepared.

Mechanistic Study of Cubane Cluster Formation. Because few mechanistic studies of cluster formation have been undertaken, we decided to examine the kinetics of conversion of our sulfur dimers to cubane clusters. Monitoring the disappearance of the PMe_3-substituted complex $Cp^*Ir(PMe_3)(\mu\text{-}S)_2IrCp^*$ (**3**) over a period of days by ^1H NMR spectroscopy demonstrated a rapid decrease in the rate of reaction. This kinetic behavior was found to be inconsistent with first- or second-order behavior. Furthermore, addition of 1 equiv of PMe_3 to complex **3** completely inhibited cubane formation even at 150 °C. Thus, the production of cubane **10** from the PMe_3 sulfido complex **3** is inhibited by the PMe_3 produced during the course of the reaction. This led us to conclude that the first step in the formation of the cubane complex **10** is reversible loss of phosphine to generate a doubly unsaturated intermediate $Cp^*Ir(\mu\text{-}S)_2IrCp^*$ (**16**), which reacts further to form the cubane complex **10** (Scheme 6). The cubane complex forms in an irreversible final step, since heating **10** with excess PMe_3 to 150 °C for several days led to no reversion to complex **3**.

A possible mechanism in the formation of other cubane complexes is generation of a monomeric $Cp^*M{=}S$ fragment which self-assembles into a cubane cluster. We can rule out this possibility in the case of **3** because heating the rhodium/iridium sulfido complex **12** led only to the production of Rh_2Ir_2 cubane **13** as supported by ^1H and $^{13}C\{^1H\}$ NMR spectroscopy, and mass spectroscopy: no Ir_4, $RhIr_3$, Rh_3Ir, or Rh_4 cubane complexes were observed. This is good evidence that the reaction maintains intact binuclear units and is not the result of initial cleavage to monomeric metal–sulfur fragments followed by condensation.

Two other important mechanistic alternatives can be distinguished kinetically. It is possible (a) that the doubly unsaturated sulfido intermediate **16** dimerizes to give the cubane **10** or (b) that **16** attacks a molecule of starting material to give cubane **10** with loss of a second phosphine (Scheme 6). A full analytical solution of the kinetics (especially for mechanism a) is complicated, but the situation is simplified under limiting (low or high) concentrations of PR_3. If at low $[PR_3]$ k_3 or k_3' in Scheme 6 is larger than $k_2[PR_3]$, both mechanisms predict a

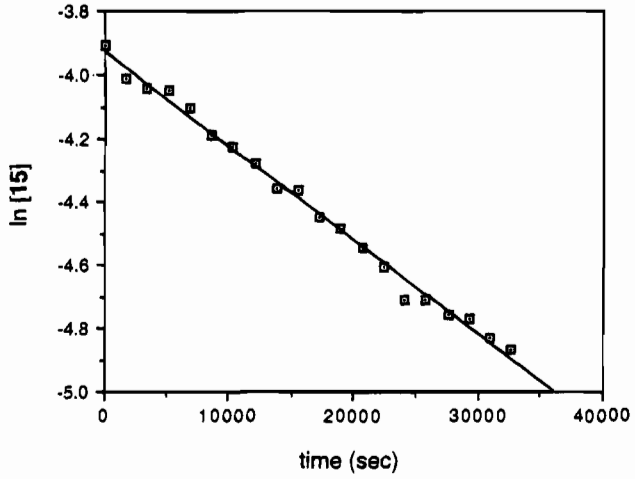

Figure 4. Representative first-order plot for the depletion of **15** ($[15]_0 = 2.0 \times 10^{-2}$ M) with no added P(*p*-tolyl)3.

rate law that is first-order in starting complex **3** and zero-order in phosphine. The key to the differentiation of the two mechanistic possibilities is rapid reversibility of step 1 at high $[PR_3]$ (i.e., $k_2[PR_3] \gg k_3$ or k_3'). Under these conditions, mechanism a leads to rate law (1), which predicts inverse second-order behavior in $[PR_3]$, and mechanism b leads to rate law (2), which predicts inverse first-order behavior in $[PR_3]$.

mechanism a

$$\text{rate} = \frac{k_3 k_1^{\,2}[Cp^*Ir(PR_3)S_2IrCp^*]^2}{k_2^{\,2}[PR_3]^2} \qquad (1)$$

mechanism b

$$\text{rate} = \frac{k_3' k_1[Cp^*Ir(PR_3)S_2IrCp^*]^2}{k_2[PR_3]} \qquad (2)$$

Because the cubane-forming reaction of PMe_3 sulfido complex **3** was found to be inhibited strongly by added PMe_3, use of this complex for testing these alternative mechanistic hypotheses proved difficult. We reasoned that a complex with a larger phosphine ligand would result in a reaction which would show diminished inhibition by phosphine ($k_2[PR_3]$ would be slower than in the corresponding reaction of the PMe_3-containing sulfido complex **3**). We therefore examined the *p*-tolylphosphine adduct **15**. Heating **15** to 60 °C for 10 h produced the cubane complex **10** and free P(*p*-tolyl)$_3$. For reactions with no added phosphine (low [P(*p*-tolyl)$_3$]), the depletion of **15** was monitored; plots of ln [**15**] versus time produced straight lines, indicating the reaction is first-order in starting material (Figure 4). This result is consistent with either mechanism a or b (eqs 1 or 2) at the low [P(*p*-tolyl)$_3$] extreme (Scheme 6).

We then carried out several runs at high, but variable, concentrations of P(*p*-tolyl)$_3$. Under these conditions, the rate was no longer first-order in [**15**]. Instead, plots of $[\mathbf{15}]^{-1}$ versus time produced straight lines indicating second-order behavior in starting material (Figure 5). Again, this result is consistent with either mechanistic alternative. However, the measured second-order rate constants k_{obs} determined from these measurements of the depletion of **15** were found to be *dependent inversely on the square* of the concentration of added P(*p*-tolyl)$_3$ (Figure 5; a plot of ln k_{obs} vs ln [P(*p*-tolyl)$_3$] showing a slope of 2 is included in the supplementary materials). That is, the rate law is that given in eq 1, with the pseudo-second-order-rate constant k_{obs} containing an inverse squared term in phos-

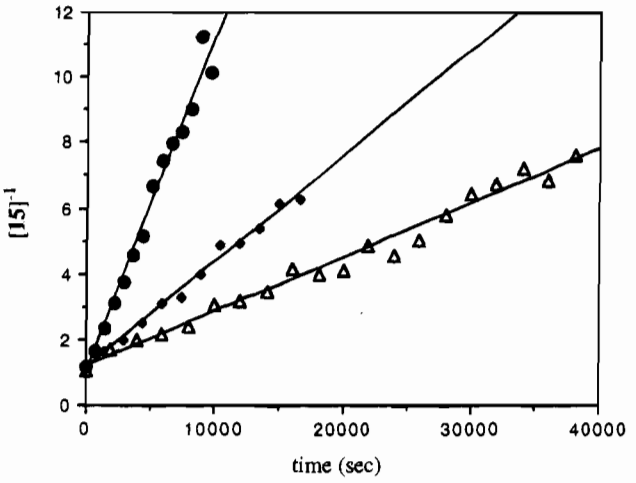

Figure 5. Dependence of k_{obsd} on the concentration of added P(*p*-tolyl)$_3$ in the thermolysis of **15** ([**15**]$_0$ 7.2 × 10^{-3} M) at 90 °C: (●) [P(*p*-tolyl)$_3$] = 0.129 M, k_{obsd} = 1.0 × 10^{-3} M^{-1} s^{-1}; (♦) [P(*p*-tolyl)$_3$] = 0.240 M, k_{obsd} = 3.2 × 10^{-4} M^{-1} s^{-1}; (△) [P(*p*-tolyl)$_3$] = 0.298 M, k_{obsd} = 1.7 × 10^{-4} M^{-1} s^{-1}. The standard deviations of the slopes of the lines are ≤3.2%.

phine. These results clearly indicate that formation of the cubane complexes involves dimerization of doubly unsaturated intermediates **16** (path a) and decisively rules out path b.

Summary

Pursuant to our goal of studying late transition-metal sulfido complexes and their states of aggregation, bimetallic iridium and mixed iridium/rhodium sulfido complexes were prepared. The sulfur bridges in these complexes were found to be nucleophilic and undergo reaction with methyl bromide. Although these complexes were found to be stable with only one metal atom occupied by phosphine, carbon monoxide and *tert*-butyl isocyanide were found first to bind to the vacant iridium atom and subsequently to replace the bound phosphine forming dimeric complexes with ligands on each of the iridium centers. Finally, we have described the formation of metal cubane clusters. Through kinetic studies and the observation that the reaction of a mixed rhodium/iridium sulfido complex produced only a dirhodium/diiridium cubane complex, we conclude that cubane formation is the result of dimerization of two doubly-unsaturated intermediates.

Experimental Section

General Considerations. Unless otherwise noted, all reactions and manipulations were performed in dry glassware under a nitrogen atmosphere in a Vacuum Atmospheres 553-2 drybox equipped with an MO-40-2 Dri-train or by using standard Schlenk techniques on a high-vacuum line. All ^1H, $^{13}C\{^1H\}$, and $^{31}P\{^1H\}$NMR spectra were recorded on one of the following instruments: a 300-MHz Fourier transform instrument constructed by Mr. Rudi Nunlist at the University of California, Berkeley, NMR facility, Bruker AMX-300 or AMX-400 spectrometers, or a Bruker AM-400 spectrometer. Coupling constants are given in hertz. The labeling scheme for the *p*-tolylphosphine aryl group is as follows:

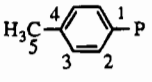

Infrared spectra were recorded on either a Nicolet 510 Fourier transform spectrometer or on a Mattson Galaxy Series FTIR 3000 spectrometer, and infrared absorptions are reported in cm^{-1}. Elemental analyses were performed at the University of California, Berkeley, Microanalysis Facility. Mass spectral analyses were performed by the University of California, Berkeley, Mass Spectrometry Laboratory on AEI-MS12 and Kratos MS-50 instruments. Molar conductivity measurements were recorded on a Fisher Scientific Co. conductivity meter in acetonitrile solution.

Benzene, diethyl ether, hexanes, pentane, THF, C_6D_6, d_8-toluene, d_8-THF, and toluene were distilled from sodium/benzophenone. Acetonitrile, d_3-acetonitrile, and d_2-methylene chloride were distilled from CaH_2. Ethanol was dried over $Ca(OEt)_2$ and stored over 3 Å molecular sieves. Cp*Ir≡N-*t*-Bu,[24] Cp*Ir(PMe$_3$)(SH)(H),[37] Cp*Rh(PMe$_3$)(SH)$_2$,[39] Cp*Ir(PMe$_3$)(SH)$_2$,[37] Cp*Ir(PMe$_3$)Cl$_2$[40] and Cp*Ir(P(*p*-tolyl)$_3$)Cl$_2$[40] were synthesized by literature procedures. Celite (diatomaceous earth) was dried overnight *in vacuo* at 200 °C. Alumina III was prepared by drying neutral alumina overnight at 200 °C *in vacuo* followed by charging with 5% water by weight and shaking vigorously. All other reagents were used as received from commercial suppliers. Reactions involving gases or low boiling liquids were performed by condensation of a known pressure of gas from a bulb of known volume into the reaction mixture. In the case of carbon monoxide, the vessel was cooled to 77 K and was charged with a known volume of gas. All manipulations were performed at room temperature unless otherwise noted. The vessel referred to below as a "bomb" is a glass vessel sealed to a Kontes vacuum adapter.

Cp*Ir(PMe$_3$)(SH)(Cl) (1). To a 20-mL flask was added 283 mg (0.647 mmol) of Cp*Ir(PMe$_3$)SH(H) and 10 mL of diethyl ether. To this solution was added by syringe 125 μL of CCl_4. The solution changed color to orange and, within 5 min, crystals formed. These were isolated by filtration and washed with 5 mL of diethyl ether, and the excess solvent was removed *in vacuo* for 1 h at 15 mTorr. This gave 230 mg (0.487 mmol, 75%) of pure **1**: ^1H NMR (C_6D_6) δ 1.42 (d, *J* = 2.0 Hz, 15H, C_5Me_5), 1.33 (d, *J* = 10.8 Hz, 9H, P*Me*$_3$), −1.13 (d, *J* = 3.7 Hz, 1H, S*H*); $^{13}C\{^1H\}$ NMR (C_6D_6) δ 91.9 (d, *J* = 3.7 Hz, *C*$_5$Me$_5$), 13.9 (d, *J* = 40.6 Hz, P*Me*$_3$), 8.73 (s, C$_5$*Me*$_5$); $^{31}P\{^1H\}$ NMR (C_6D_6) δ −32.7; IR (KBr) 2975 (s), 2912 (s), 2512 (m), 1450 (m), 1412 (s), 1275 (s), 1031 (m), 956 (s). Anal. Calcd for $C_{13}H_{25}IrPSCl$: C, 33.08; H, 5.34. Found: C, 33.23; H, 5.30.

Cp*Ir(PMe$_3$)(μ-S)$_2$IrCp* (3). A 50-mL flask was charged with 500 mg (1.05 mmol) of Cp*Ir(PMe$_3$)Cl$_2$ and 15 mL of acetonitrile. To this orange suspension was added 206 mg (2.64 mmol) of Na_2S, and the resulting suspension was stirred at room temperature for 36 h, during which time the color changed from orange to dark green. The mixture was filtered through a 2 cm × 2 cm pad of Celite, and the volatile materials were removed *in vacuo* for 2 h at 15 mTorr. The product was purified by dissolving the product in 50 mL of hexane, transferring the resulting solution onto a 2.5 cm × 15 cm neutral alumina III column, and eluting with 15% THF/ hexanes. A green band was eluted first and collected. Removal of the solvent *in vacuo* for 2 h at 15 mTorr gave 302 mg (0.380 mmol, 72%, judged pure by ^1H NMR spectroscopy) of green microcrystals. The compound was recrystallized from diethyl ether at −40 °C in order to obtain an analytically pure sample: ^1H NMR (C_6D_6) δ 1.72 (s, 15H, C$_5$*Me*$_5$), 1.72 (d, *J* = 2.0 Hz, 15H, C$_5$*Me*$_5$-Ir(P)), 1.55 (d, *J* = 10.2 Hz, 9H, P*Me*$_3$); $^{13}C\{^1H\}$ NMR (C_6D_6) δ 92.6 (d, *J* = 3.6 Hz, *C*$_5$Me$_5$Ir(P)), 85.8 (s, *C*$_5$Me$_5$), 14.9 (d, *J* = 39.4 Hz, P*Me*$_3$), 10.0 (s, C$_5$*Me*$_5$), 8.92 (s, C$_5$*Me*$_5$); $^{31}P\{^1H\}$ NMR (C_6D_6) δ −37.8; IR (KBr) 2969 (s), 2903 (s), 950 (s). Anal. Calcd for $C_{23}H_{39}Ir_2PS_2$: C, 34.75; H, 4.94. Found: C, 34.45; H, 4.97.

Crystal Structure Determination of Cp*Ir(PMe$_3$)(μ-S)$_2$IrCp* (3). Green crystals of **3** were obtained from a concentrated diethyl ether solution cooled to −40 °C. A single crystal was mounted in Paratone N hydrocarbon oil. The crystal was then transferred to an Enraf-Nonius CAD-4 diffractometer, centered in the beam, and cooled by a nitrogen-flow low-temperature apparatus. The final cell parameters and specific collection parameters are given in Table 1. The 1894 raw intensity data were converted to structure factor amplitudes and their esd's by correction for scan speed, background, and Lorentz and polarization effects. No correction for crystal decay was necessary. Space group $P2_1$ was confirmed by refinement. The structure was solved by Patterson methods and refined via standard least-squares and Fourier techniques. Only the iridium, sulfur, and phosphorous atoms were refined with anisotropic thermal parameters. An attempt to refine the anisotropic thermal parameters of all carbons led to unrealistic values.

(40) Kang, J. W.; Moseley, K.; Maitlis, P. M. *J. Am. Chem. Soc.* **1969**, *91*, 5970−5980.

Cp2 showed obvious signs of disorder, which was modeled with fully occupied C11, C12, C13, and C17, $^2/_3$ occupancy for C14, C14′, and C15, and $^1/_2$ occupancy for C16, C16′, and C18-C20′. The PMe_3 carbons refined properly with anisotropic thermal parameters but Cp1 did not refine properly and so was refined with isotropic thermal parameters. The final residuals for **3** are given in Table 1.

The quantity minimized by the least-squares program was $\sum w(|F_o| - |F_c|)^2$, where w is the weight of a given observation. The p-factor used to reduce the weight of intense reflections was set to 0.03 throughout the refinement. The analytical forms of the scattering factor tables for neutral atoms were used, and all scattering factors were corrected for both the real and imaginary components of anomalous dispersion.

Cp*Ir(PMe$_3$)(μ-S)$_2$IrCp* (3) from Cp*Ir(PMe$_3$)SH(Cl) (1). To a 25-mL flask was added 40 mg (0.085 mmol) of Cp*Ir(PMe_3)SH(Cl) and 6 mL of toluene. To this solution was added 22 mg (0.11 mmol) of potassium hexamethyldisilazane in 1 mL of toluene. The solution became red instantaneously and after 2 h was green. After cooling of the solution to −40 °C for 2 h, the resulting mixture was filtered successively through a 2 cm × 2 cm pad of Celite and a 2 cm × 2 cm pad of alumina III. The volatile materials were removed *in vacuo* for 4 h at 15 mTorr giving 34 mg (0.085 mmol, 99%) of a green complex. A ^{1}H NMR spectrum confirmed compound **3** was the only proton containing product.

[Cp*Ir(PMe$_3$)(μ-SMe)$_2$Ir(Br)Cp*]Br (4). A 25-mL flask was charged with 94 mg (0.118 mmol) of **3** and 20 mL of benzene. The flask was cooled to 77 K and charged with methyl bromide (0.486 mmol, 65 Torr/139.2 mL at 298 K) by vacuum transfer. The solution changed from dark green through a deep reddish color to transparent yellow. Removal of the volatile materials *in vacuo* for 2 h at 15 mTorr gave 104 mg (0.105 mmol, 89%) of a yellow solid: ^{1}H NMR (CD_3CN) δ 2.05 (s, 6H, S*Me*), 1.86 (d, J = 2.5 Hz, 15H, C_5Me_5Ir(P)), 1.70 (d, J = 11.0 Hz, 9H, P*Me*$_3$), 1.60 (s, 15H, C_5Me_5); ^{13}C{^{1}H} NMR (CD_3CN) δ 98.5 (d, J = 2.7 Hz, C_5Me_5Ir(P)), 91.2 (s, C_5Me_5), 15.3 (s, S*Me*), 13.0 (d, J = 41.0 Hz, P*Me*$_3$), 10.5 (s, C_5Me_5), 9.12 (s, C_5Me_5); ^{31}P{^{1}H} NMR (CD_3CN) δ −2.71; Ir (KBr) 2917 (m), 948 (s). Molar conductivity, Λ_m: 147 Ω^{-1} cm^2 mol^{-1}. Anal. Calcd for $C_{25}H_{45}Ir_2Br_2PS_2$: C, 30.49; H, 4.61. Found: C, 30.08; H, 4.47.

Cp*Ir(PMe$_3$)(μ-SMe)(μ-S)Ir(Br)Cp* (5). A 25-mL flask was charged with 113 mg (0.142 mmol) of **3** and 7 mL of benzene. The flask was cooled to 77 K and charged with methyl bromide (0.135 mmol, 38 Torr/66.3 mL at 298 K) by vacuum transfer. The solution changed from green to a deep reddish color. After 24 h at room temperature, 98 mg of deep red crystals was collected which was found to be contaminated by **4** (89% yield of **5** by ^{1}H NMR spectroscopy, 10:1 mixture of **5**:**4**). This mixture could not be separated. Data for **5**: ^{1}H NMR (CD_3CN) δ 2.36 (s, 3H, S*Me*), 1.69 (s, 15H, C_5Me_5), 1.65 (d, J = 1.8 Hz, 15H, C_5Me_5Ir(P)), 1.60 (d, J = 10.4 Hz, 9H, P*Me*$_3$); ^{13}C{^{1}H} NMR (CD_3CN) δ 96.3 (d, J = 2.8 Hz, C_5Me_5Ir(P)), 91.1 (s, C_5Me_5), 18.6 (s, S*Me*), 16.3 (d, J = 40.1 Hz, P*Me*$_3$), 10.3 (s, C_5Me_5), 8.63 (s, C_5Me_5).

Cp*Ir(PMe$_3$)(μ-S)$_2$Ir(CO)Cp* (6). A 10-mL flask was charged with 94 mg (0.12 mmol) of **3** and 5 mL of benzene and was equipped with a vacuum adapter. This solution was cooled to 77 K, and 1.0 mmol of CO was added (430 Torr/13 mL). The green solution was warmed to room temperature for 20 min during which time the color changed to red. Removal of volatile materials *in vacuo* for 2 h at 15 mTorr gave 95 mg (0.12 mmol, 99%) of a red microcrystalline solid: ^{1}H NMR (C_6D_6) δ 1.81 (d, J = 1.8 Hz, 15H, C_5Me_5Ir(P)), 1.71 (s, 15H, C_5Me_5), 1.57 (d, J = 10.5 Hz, 9H, P*Me*$_3$); ^{13}C{^{1}H} NMR (C_6D_6) δ 178.9 (s, *C*O), 100.1 (s, C_5Me_5), 95.5 (d, J = 3.8 Hz, C_5Me_5Ir(P)), 16.4 (d, J = 42.0 Hz, P*Me*$_3$), 9.28 (s, C_5Me_5), 8.62 (s, C_5Me_5); ^{31}P{^{1}H} NMR (C_6D_6) δ −22.5; IR (KBr) 2906 (m), 1968 (s), 1451 (s), 945 (s). Anal. Calcd for $C_{24}H_{39}Ir_2OPS_2$: C, 35.02; H, 4.78. Found: C, 34.85; H, 4.70.

Cp*Ir(CO)(μ-S)$_2$Ir(CO)Cp* (7). To a 15-mL bomb was added 134 mg (0.169 mmol) of Cp*Ir(PMe_3)S_2IrCp* and 8 mL of benzene. This vessel was cooled to 77 K and charged with 530 Torr of carbon monoxide and heated at 85 °C for 2 days. After the sample was cooled to room temperature, 18 mg of analytically pure crystals was collected from the reaction mixture by filtration. Removal of the volatile materials *in vacuo* from the mother liquor for 2 h at 15 mTorr combined with the crystals isolated gave 110 mg (0.142 mmol, 84%) of **7** judged pure by ^{1}H NMR spectroscopy: ^{1}H NMR (CD_2Cl_2) δ 1.91 (s, C_5Me_5); ^{13}C{^{1}H} NMR (CD_2Cl_2) δ 176.4 (s, *C*O), 101.6 (s, C_5Me_5), 8.76 (s, C_5Me_5); IR (KBr) 2917 (s), 1974 (s). Anal. Calcd for $C_{22}H_{30}Ir_2O_2S_2$: C, 34.10; H, 3.90. Found: C, 33.81; H, 3.81.

Cp*Ir(PMe$_3$)(μ-S)$_2$Ir(CN-*t*-Bu)Cp* (8). This complex was identified as an intermediate in the reaction of **3** with *tert*-butyl isocyanide and could not be isolated: ^{1}H NMR (C_6D_6) δ 1.90 (d, J = 1.8 Hz, 15H, C_5Me_5Ir(P)), 1.79 (s, 15H, C_5Me_5), 1.67 (d, J = 10.5 Hz, 9H, P*Me*$_3$), 1.38 (s, 9H, C*Me*$_3$).

Cp*Ir(CN-*t*-Bu)(μ-S)$_2$Ir(CN-*t*-Bu)Cp* (9). To a 50-mL flask was added 111 mg (0.139 mmol) of Cp*Ir(PMe_3)S_2IrCp* and 20 mL of benzene. This vessel was cooled to 77 K and charged with *tert*-butyl isocyanide (0.306 mmol, 41 Torr/139.2 mL at 298 K) via vacuum transfer and heated at 80 °C for 2 days. The volatile materials were removed *in vacuo* to give an orange powder which was slurried in hexanes, placed on a glass frit, washed with two 5-mL portions of hexanes, and washed through the frit with 10 mL of toluene. Removal of the solvent gave 102 mg (0.115 mmol, 83%) of **9**: ^{1}H NMR (C_6D_6) δ 1.95 (s, 15H, C_5Me_5), 1.31 (s, 9H, C*Me*$_3$); ^{13}C{^{1}H} NMR (C_6D_6) δ 183.1 (s, *C*NCMe$_3$), 96.7 (s, *C*$_5$Me$_5$), 55.8 (s, CN*C*Me$_3$), 32.1 (s, CNC*Me*$_3$), 9.01 (s, C_5Me_5); IR (KBr) 2973 (m), 2919 (s), 2855 (m), 2112 (s), 2069 (s), 1372 (m), 1208 (m). Anal. Calcd for $C_{30}H_{48}Ir_2N_2S_2$: C, 40.70; H, 5.47; N, 3.16. Found: C, 40.46; H, 5.49; N, 3.37.

Crystal Structure Determination of Cp*Ir(CN-*t*-Bu)(μ-S)$_2$Ir(CN-*t*-Bu)Cp* (9). Red crystals of **9** were obtained from a toluene solution into which pentane was vapor diffused at room temperature. A single crystal was mounted as described for **3**. The final cell parameters and specific collection parameters are given in Table 1. The 4852 raw intensity data were converted to structure factor amplitudes and their esd's by correction for scan speed, background, and Lorentz and polarization effects. No correction for crystal decay was necessary. Space group *C*2/*c* was confirmed by refinement. The structure was solved by Patterson methods and refined via standard least-squares and Fourier techniques. All non-hydrogen atoms were refined with anisotropic thermal parameters. The final residuals for **9** are given in Table 1. Minimization was carried out as for **3**.

(Cp*IrS)$_4$ (10). Into a 20-mL bomb was placed 34 mg (0.043 mmol) of **3** and 10 mL of benzene. This solution was heated to 135 °C for 24 h, and then removed from heat and the volume was reduced by 50% *in vacuo* to remove PMe_3. A 5-mL volume of benzene was then added, and the solution was heated to 135 °C. This was repeated for each of 7 days. The resulting red solution was slowly cooled to room temperature during which time crystals formed. These were isolated by filtration and excess solvent was removed *in vacuo* for 2 h at 15 mTorr to gave 20 mg (0.028 mmol, 65%) of red crystals: ^{1}H NMR (C_6D_6) δ 1.71 (s); ^{13}C{^{1}H} NMR (C_6D_6) δ 88.7 (s, C_5Me_5), 7.93 (s, C_5Me_5); IR (KBr) 2966 (m), 2910 (s), 1447 (m), 1370 (s), 1032 (s). Anal. Calcd for $C_{40}H_{60}Ir_4S_4$: C, 33.41; H, 4.21. Found: C, 33.49; H, 3.76.

Crystal Structure Determination of (Cp*IrS)$_4$ (10). Red crystals of **10** were obtained from a 135 °C benzene solution slowly cooled to 25 °C. A single crystal was mounted as described for **3**. The 2781 raw intensity data were converted to structure factor amplitudes and their esd's by correction for scan speed, background, and Lorentz and polarization effects. No correction for crystal decay was necessary. The structure was solved by Patterson methods and refined via standard least-squares and Fourier techniques. Only the iridium and sulfur atoms were refined with anisotropic thermal parameters. The data were initially collected in a triclinic primitive space group, but the data were then transformed to the body-centered tetragonal cell. Inspection of the azimuthal scan data showed the possibility of systematic error in that data, so the transformed tetragonal data were refined against an isotropic model including hydrogen atom predicted positions. The data were corrected for "absorption" via the program DIFABS and then averaged. This improved the averaging statistics from R_I = 6.4% to R_I = 4.7%. However, attempts to refine the carbon atoms with anisotropic thermal parameters led consistently to one or two of them having irrational values (the tensor became non-positive-definite) and the rest showing a saucer-like shape. The final refinement includes hydrogen atoms in predicted positions and refinement of carbon atoms

with isotropic thermal parameters. The final cell parameters and specific collection parameters are given in Table 1. The final residuals for **9** are given in Table 1.

Cp*Rh(PMe$_3$)(μ-S)$_2$IrCp* (12). A 20-mL flask was charged with 72 mg (0.181 mmol) of Cp*Ir≡N-*t*-Bu, 68.7 mg (0.181 mmol) of Cp*Rh(PMe$_3$)(SH)$_2$, 10 mL of diethyl ether, and 1 mL of toluene. This solution was stirred for 1 h at room temperature and the volatile materials were removed *in vacuo* for 2 h at 15 mTorr. The crude product was crystallized from a minimum amount of diethyl ether at −40 °C in two crops and gave 119 mg (0.168 mmol, 93%) of brown-green crystals: ^{1}H NMR (C_6D_6) δ 1.71 (d, J = 2.4 Hz, 15H, C_5Me_5-Rh), 1.69 (s, 15H, C_5Me_5), 1.47 (d, J = 10.1 Hz, 9H, PMe_3); ^{13}C{^{1}H} NMR (C_6D_6) δ 97.2 (vt, J = 3.9 Hz, C_5Me$_5$Rh), 86.0 (s, C_5Me$_5$Ir), 16.2 (d, J = 32.8 Hz, PMe_3), 10.1 (s, C_5Me_5), 9.5 (s, C_5Me_5); ^{31}P{^{1}H} NMR (C_6D_6) δ −7.82 (d, J = 165.9 Hz); IR (KBr) 2967 (m), 2898 (s), 1448 (m), 1372 (s), 1025 (m), 949 (s). Anal. Calcd for $C_{23}H_{39}$-IrPRhS$_2$: C, 39.14; H, 5.57. Found: C, 39.32; H, 5.61.

(Cp*IrS)$_2$(Cp*RhS)$_2$ (13). In a 20-mL bomb was placed 360 mg (0.510 mmol) of **12** and 7 mL of benzene. This solution was heated to 120 °C for 16 h and slowly cooled to room temperature during which time crystals formed. These were isolated by filtration, and excess solvent was removed *in vacuo* for 2 h at 15 mTorr to give 171 mg (0.270 mmol, 53%) of dark red crystals: ^{1}H NMR (C_6D_6) δ 1.74 (s, 15H, C_5Me_5), 1.69 (s, 15H, C_5Me_5); ^{13}C{^{1}H} NMR (C_6D_6) δ 93.9 (d, J = 4.8 Hz, C_5Me$_5$Rh), 88.0 (s, C_5Me$_5$Ir), 8.72 (s, C_5Me_5), 8.24 (s, C_5Me_5); FAB MS *m/e* 1260 (MH$^+$); IR (KBr) 2968 (m), 2903 (s), 1450 (m), 1371 (s), 1153 (m), 1028 (s). Anal. Calcd for $C_{40}H_{60}Ir_2Rh_2S_4$: C, 38.15; H, 4.80. Found: C, 38.64; H, 4.81. Several attempts were made at elemental analysis. The reported value is the best obtained.

Cp*Ir(P(*p*-tolyl)$_3$)(SH)$_2$ (14). To a 50-mL flask equipped with a vacuum adapter was added 210 mg (0.299 mmol) of Cp*Ir(P(*p*-tolyl)$_3$)-Cl$_2$ and 50 mg (0.892 mmol) of sodium hydrogen sulfide. This solid mixture was cooled to 77 K, and 20 mL of ethanol was added via vacuum transfer. Into the frozen solution was vacuum transferred 8.42 mmol of hydrogen sulfide (310 Torr/505 mL at 298 K), and the resulting mixture was warmed to room temperature. The reaction mixture was stirred at room temperature for 3 days. Removal of the volatile materials *in vacuo* for 2 h at 15 mTorr, extraction with 20 mL of toluene, filtration through Celite and removal of the solvent *in vacuo* for 2 h at 15 mTorr gave 191 mg (0.274 mmol, 91.5% crude) of a yellow powder. This compound was found to be thermally sensitive and was used as soon as prepared: ^{1}H NMR (CD_2Cl_2) δ 7.42 (br s, 6H, MeC$_6H_4$P), 7.16 (br d, J = 6.7 Hz, 6H, MeC$_6H_4$P), 2.37 (s, 9H, *Me*C$_6$H$_4$P), 1.41 (d, J = 2.1 Hz, 15H, C_5Me_5), −2.41 (d, J = 4.7 Hz, 2H, S*H*); ^{13}C{^{1}H} NMR (CD_2Cl_2) δ 140.5 (br s, C4), 135.1 (d, J = 9.8 Hz, C2), 129.7 (br d, J = 43.9 Hz, C1), 128.5 (br d, J = 10.3, C3), 94.6 (d, J = 3.1 Hz, C_5Me$_5$), 21.3 (s, C5), 8.3 (d, J = 1.0 Hz, C_5Me_5); ^{31}P{^{1}H} NMR (CD_2Cl_2) δ 0.0; IR (KBr) 2917 (s), 1496 (s), 1447 (m), 1096 (s), 808 (m), 527 (s).

Cp*Ir(P(*p*-tolyl)$_3$)(μ-S)$_2$IrCp* (15). A 50-mL flask was charged with 506 mg of freshly prepared **14** (0.725 mmol), 289 mg (0.725 mmol) of Cp*Ir≡N-*t*-Bu, and 20 mL of benzene. The resulting mixture was stirred for 2 days. Removal of the volatile materials *in vacuo* for 12 h at 15 mTorr and crystallization of the green solid from a minimum amount of toluene layered with pentane gave 798 mg (0.682 mmol, 94%) of green crystals: ^{1}H NMR (d_8-THF) δ 7.49 (dd, J_1 = 10.3 Hz, J_2 = 8.1 Hz, 6H, MeC$_6H_4$P), 7.03 (br d, J = 8.1 Hz, 6H, MeC$_6H_4$P), 2.32 (s, 9H, *Me*C$_6$H$_4$P), 1.57 (s, 15H, C_5Me_5), 1.36 (d, J = 1.7 Hz, C_5Me_5Ir(P)); ^{13}C{^{1}H} NMR (d_8-THF) δ 139.1 (s, C4), 135.8 (d, J = 10.0 Hz, C2), 132.3 (d, J = 56.6 Hz, C1), 128.0 (d, J = 10.4 Hz, C3), 94.7 (d, J = 3.6 Hz, C_5Me$_5$Ir(P)), 86.1, (s, C_5Me$_5$), 21.3 (s, C5), 10.1 (s, C_5Me_5), 8.5 (s, C_5Me_5); ^{31}P{^{1}H} NMR (d_8-THF) δ 9.5; IR (KBr) 2904 (s), 1499 (m), 1450 (s), 1093 (m), 1028 (m), 530 (s). Anal. Calcd for $C_{41}H_{51}Ir_2PS_2$: C, 48.12; H, 4.81. Found: C, 48.27; H, 4.97.

Kinetics. All kinetic experiments were monitored by ^{1}H NMR spectroscopy in C_6D_6 at 90 °C using a Bruker AMX-400 MHz NMR spectrometer. Standard solutions of compound **15** were prepared in the drybox using volumetric pipets and stored in a −40 °C freezer. Individual samples were prepared by transferring this material with volumetric pipets into a 10-mL vial in which P(*p*-tolyl)$_3$ was weighed previously. The resulting solution was transferred to a new dry 8-in. Wilmad NMR tube. The internal standard (*p*-dimethoxybenzene) dissolved in C_6D_6 to produce a standard solution was then added via syringe. A metal Cajon adapter connected to a Kontes high vacuum stopcock was employed, and the solution was frozen (77 K) and sealed. The sample was placed into the NMR spectrometer, and the initial concentrations were measured. The NMR tube was removed, the NMR probe was heated to 90 ± 0.5 °C, and the sample was replaced and allowed to equilibrate. Data were collected using the TIME RUN program written by Mr. Rudi Nunlist of the University of California, Berkeley, NMR Facility. The temperature was calibrated using ethylene glycol.[41]

Reactions were monitored by observing the growth of the resonance at δ 1.71 ppm for the pentamethylcyclopentadienyl ligand of the product, (Cp*IrS)$_4$ (**10**), or by monitoring the loss of the resonance at δ 2.32 ppm of **15** by single pulse ^{1}H NMR spectroscopy experiments. Plots of ln (concentration) versus time were plotted and fitted to infinity values using a data manipulation program created by Dr. Kevin Kyle of this laboratory using IGOR software. Runs were monitored for at least 3 half-lives. Plots of (concentration)$^{-1}$ versus time were plotted using the CRICKETGRAPH program.

Acknowledgment. We are grateful for support of this work from the National Science Foundation (Grant No. CHE-9113261). We also acknowledge a gift of iridium chloride from the Johnson-Matthey Aesar/Alfa metal loan program. We would like to thank Dr. F. J. Hollander for determination of the crystal structures of complexes **3**, **10**, and **13**, Mr. Mike Perrot for determination of the crystal structure of complex **9**, and Dr. Bruce A. Arndtsen for assistance with plotting kinetic data.

Supplementary Material Available: X-ray diffraction data (tables of positional, isotropic, and anisotropic thermal parameters, least-squares planes, dihedral angles, and full interatomic distances and angles) for **3**, **9**, and **10** and a plot of k_{obs} values vs [P(*p*-tolyl)$_3$] (13 pages). This is provided with the archival edition of the journal, available in many libraries. Alternatively, ordering information is given on any current masthead page.

(41) Raiford, D. S.; Fisk, C. L.; Becker, E. D. *Anal. Chem.* **1979**, *51*, 2050–2051.